Advances in Process Simulation of Agglomeration in Bayer Precipitation

Ab Rijkeboer[1], John McFeaters[2] and Daniel Manché[3]

1. Director, Rinalco BV, Wassenaar, The Netherlands
2. Director, US Office, KWA Kenwalt Australia Pty Ltd, Baton Rouge, LA, USA
3. Simulation Engineer, Europe Office, KWA Kenwalt Australia Pty Ltd, Lisbon, Portugal

Corresponding author: ab@rinalco.com

Abstract

Developing a Bayer precipitation circuit model with accurate predictive capability requires comprehensive physical models for the fundamental processes occurring and, importantly, a structured approach to tuning the model to available plant data. A new agglomeration size kernel has been constructed based on agglomeration kernels developed by René David et al. for different types of eddies within turbulence. The new kernel takes account of the fact that two types of eddies are of practical relevance to agglomeration in precipitation circuits, namely small laminar eddies whose behaviour is dominated by viscous forces and larger eddies whose behaviour is dominated by inertial forces. As well as simulating the chemical and physical processes underlying agglomeration, the kernel offers flexibility in its application due to the inclusion of various adjustable parameters. This facilitates model calibration for accurate prediction of particle size distribution (PSD) in the discharge flows from tanks in the precipitation circuit where complex particle interactions take place under a variety of hydrodynamic conditions. The kernel has been implemented into the Precipitator 3 unit model of the SysCAD process simulation software. A systematic procedure for calibration has been developed for obtaining the closest approach to the target PSD whereby various combinations of kernel parameters are tested with simultaneous tuning of constants for growth, nucleation, and agglomeration rates on their respective targets. Aspects of supersaturation, growth rate, nucleation rate and agglomeration rate are reviewed in the context of calibrating predictive established relationships.

Keywords: Process simulation, Agglomeration, Nucleation, Growth, Calibration.

1. Introduction

Product quality and production rate are ongoing concerns in alumina refineries. Uncertainties often arise about the best way to resolve product quality issues with the least impact on production or how to optimise plans for production improvements. In these cases it is useful to have a tool which can predict changes in particle size distribution (PSD) around the white-side circuit as a consequence of changes in operating parameters, circuit configuration or equipment conditions.

Recently a new agglomeration size kernel has been added to the SysCAD process simulation software. The kernel offers a large degree of flexibility in calibrating a precipitation circuit model to an existing plant circuit such that each tank in the model has the right set of parameters producing the correct gibbsite mass with the correct PSD. This paper discusses this new kernel and the method of calibration. In this context, attention is also paid to fundamental aspects of growth rate, nucleation rate and agglomeration rate.

Agglomeration of $Al(OH)_3$ (gibbsite or hydrate) crystals in the Bayer process has been extensively studied in Australian research institutions. In the early 2000 s a collaborative research project was executed within CSIRO Minerals under the direction of AMIRA. Dean Ilievski and Iztok Livk were the leading scientists on this project and published important results, conclusions and correlations, including an agglomeration kernel that is available in SysCAD. Their experimental

work was conducted in two types of reactors: an in-house developed reactor for simulating laminar flow conditions and another for simulating turbulent flow conditions [1]. Regarding the latter it was recognised that the agitator power input, thus shear rate, per reactor volume unit was an order of magnitude greater than in real-world precipitators. To overcome this issue, the conclusions from both the laminar and turbulent reactors were considered in constructing an agglomeration kernel.

In this paper a more pragmatic approach is presented whereby the actual precipitators in a plant serve as kernel parameter development reactors. In this approach, scientific findings regarding agglomeration under laminar and turbulent flow conditions are used, but a degree of flexibility has been incorporated into the kernel to account for the actual plant environment.

2. New Agglomeration Kernel

2.1 Microscales of Turbulence

The new kernel is based on expressions from publications by René David et al. [2, 3, 4] about their research into the agglomeration of adipic acid crystals. These expressions relate to the hydrodynamic and orthokinetic conditions within the turbulence in a tank, where different types of eddies can be distinguished. Turbulent energy is added at the largest length scales. The vortices or eddies created are distorted and broken into continually smaller eddies. Of interest here are eddies at the smaller scales, where agitator energy input is ultimately dissipated as heat via viscous action. The Taylor microscale, λ_g, is the scale at which viscous effects start to become important, while turbulent inertia through flow fluctuations in magnitude and direction is still present. Below the Kolmogorov microscale, λ_k [5], viscous effects dominate and motion is laminar.

$$\lambda_k = \left(\frac{\nu^3}{\varepsilon}\right)^{1/4} \tag{1}$$

$$\lambda_g = \theta \cdot \left(\frac{60\nu}{\varepsilon}\right)^{1/2} \tag{2}$$

where:

λ_k	Kolmogorov microscale of turbulence, m
λ_g	Taylor scale of turbulence, m
ν	Kinematic viscosity, $m^2\ s^{-1}$
ε	Energy dissipation rate per unit mass, $J\ s^{-1}\ kg^{-1}$
θ	Fluctuating average component of the local velocity, $m\ s^{-1}$

The Taylor and Kolmogorov microscales are typically within the hydrate particle size range of Bayer circuit precipitators. These scales can vary from tank to tank and from location to location within a tank. It is worth noting that turbulence is a characteristic of the flow situation, not a property of the fluid, and that these scales are not exact dimensions but representative dimensions.

2.2 The Process of Agglomeration

The Kolmogorov microscale is an important transition point for particle behaviour. The motion of particles smaller than the Kolmogorov microscale is dominated by viscous forces. These particles have little motion relative to the fluid. They tend to move parallel to each other in the laminar flow elements. Collisions between these small particles only occur because particles catch up with each other as a result of a viscosity related, shear induced velocity gradient. The chance of collision as a function of particle size is described by Smoluchovski [6]. Particles larger than the Kolmogorov microscale tend to follow more diverse individual flow patterns and exhibit varied velocity fluctuations and trajectory changes. They have a much greater chance of being involved in collisions, e.g. with each other, or with the smaller particles crossing their path.

Collision is only the first step towards agglomeration; once two particles have collided they need to stay attached. There are two opposing processes taking place. One is growth at the collision interface that leads to consolidation of the bond between the two particles. The other is shear, trying to rip the two particles apart again. The higher the growth rate the higher the chance that an agglomerate survives, while for shear rate it is the reverse. It can easily be visualised that a fresh doublet of two particles of approximately the same size has a much higher chance to be ripped apart before a strong enough bond forms between them than a doublet of a small particle attached to a large particle of equivalent total diameter.

Finally, when the size of a fresh doublet approaches the Taylor microscale the survival rate diminishes with increasing size because of the increasing impact of turbulence. Above the Taylor microscale, fresh agglomerates are rapidly destroyed [2].

These observations regarding chance of collision and chance of agglomerate consolidation lead to a particular shape of kernel where the highest rate of successful agglomeration occurs between small particles and large particles up to a point where the overall size of a fresh agglomerate becomes too big for survival.

2.3 Kernel Component Expressions

David et al. [2, 3, 4] published kernels for conditions below and above the Kolmogorov microscale, thus being applicable to laminar and turbulent eddies respectively. The laminar kernel represents an expression for collision rate based on a shear induced velocity gradient which stems from a 1917 paper by Smoluchovski [6]. It has withstood the test of time and has been confirmed and used by several other scientists involved in agglomeration kernel development, including Ilievski and Livk [1].

Laminar:

$$\beta(\overline{D}_x, \overline{D}_y) = \beta_L \cdot H(\overline{D}_x, \overline{D}_y) = \beta_L \cdot (\overline{D}_x + \overline{D}_y)^3 \quad (3)$$

Turbulent:

$$\beta(\overline{D}_x, \overline{D}_y) = \beta_T \cdot H(\overline{D}_x, \overline{D}_y) = \beta_T \cdot \frac{(\overline{D}_x + \overline{D}_y)^2}{Min(\overline{D}_x, \overline{D}_y)} \cdot \left(1 - \frac{(\overline{D}_x + \overline{D}_y)^2}{\lambda_g^2}\right) \quad (4)$$

With: $(\overline{D}_x + \overline{D}_y) \leq \lambda_g$ (replacing the original Heaviside step function)

where:

$\beta(\overline{D}_x, \overline{D}_y)$	Rate at which particles from bin *x* form permanent agglomerates with particles from bin *y*.
$H(\overline{D}_x, \overline{D}_y)$	Chance that a particle from bin *x* forms a permanent agglomerate with a particle from bin *y*.
$\overline{D}_x, \overline{D}_y$	Average diameter of bin *x* and *y* respectively, m Average diameter of e.g. bin *x* defined by David et al. as ($D_{x\text{-}1}$ + D_x) / 2, with $D_{x\text{-}1}$ and D_x being the top sizes of bin(*x*-1) and bin(*x*) respectively.
β_L, β_T	Agglomeration rate factor for laminar and turbulent flow regimes, respectively, dependent on process and hydrodynamic conditions, such as growth rate, temperature, solids concentration, shear rate, viscosity.
λ_g	Taylor microscale, m

As applied in SysCAD, the term “bin” refers to size class or size interval.

Examples of Equations (3) and (4) are shown in Figures 1 and 2.

The last term in Equation (4) is described in [4] as an osculatrix parabola approximation of a Lagrangian correlation for the case of isotropic turbulence. It provides a gradual reduction in survival rate of agglomerates with increasing size until zero is reached at $\overline{D}_x + \overline{D}_y = \lambda_g$.

Below the Kolmogorov microscale is the Batchelor microscale which marks the transition from collisions determined by laminar flow conditions to collisions governed by Brownian motion (diffusion). David et al. [2] also specify a kernel applicable to Brownian motion, but this kernel is not considered herein as it concerns ultrafine particles of submicron size which fall outside the usual PSD specifications in Bayer precipitation modelling.

2.4 Combining the Expressions

In the new kernel, the laminar and turbulent kernels are combined with a smooth transition at the Kolmogorov microscale. Its value is difficult to determine from hydrodynamics in a precipitator, having different zones of turbulence. Its value is found through calibration as discussed hereafter. The transition term resembles the Rosin-Rammler particle size distribution expression:

$$\varphi = Exp\left(\ln(0.5) \cdot \left(\frac{\overline{D}_x + \overline{D}_y}{\lambda_k}\right)^{\propto}\right) = 0.5^{\left(\frac{\overline{D}_x + \overline{D}_y}{\lambda_k}\right)^{\propto}} \quad (5)$$

where:

λ_k Kolmogorov microscale of turbulence, m
α Transition sharpness, where lower value gives a more gradual transition.

The combined kernel (see Figure 3 for an example) takes the form:

$$\beta_L \cdot \varphi \cdot (\overline{D}_x + \overline{D}_y)^3 + \beta_T \cdot (1 - \varphi) \cdot \frac{(\overline{D}_x + \overline{D}_y)^2}{Min(\overline{D}_x, \overline{D}_y)} \cdot \left(1 - \frac{(\overline{D}_x + \overline{D}_y)^2}{\lambda_g^2}\right) \quad (6)$$

With: $(\overline{D}_x + \overline{D}_y) \leq \lambda_g$

This kernel covers the fundamentals of agglomeration as researched by René David et al., while being versatile in its application. It allows the user to select values for the parameters λ_g, λ_k, α, β_L and β_T that best describe the PSD changes in their agglomerators.

2.5 Final Kernel

The kernel has been made even more versatile by replacing the combined representative particle size $\overline{D}_x + \overline{D}_y$ with the generalised mean of $\overline{D}_x$ and $\overline{D}_y$ multiplied by 2.

Laminar:

$$SL_{\overline{D}_x,\overline{D}_y} = 2 \cdot \sqrt[m]{1/2 \cdot (\overline{D}_x^{\,m} + \overline{D}_y^{\,m})} \quad (7)$$

Turbulent:

$$ST_{\overline{D}_x,\overline{D}_y} = 2 \cdot \sqrt[n]{1/2 \cdot \left(\overline{D}_x^{\,n} + \overline{D}_y^{\,n}\right)}. \quad (8)$$

The following applies for both Equations (7) and (8):

$SL_{\overline{D}_x,\overline{D}_y} = \overline{D}_x + \overline{D}_y$ for m = 1 and for $\overline{D}_x = \overline{D}_y$
$SL_{\overline{D}_x,\overline{D}_y} < \overline{D}_x + \overline{D}_y$ for m < 1 while $\overline{D}_x \neq \overline{D}_y$ and the opposite applies for m > 1

Difference from the original $\overline{D}_x + \overline{D}_y$ increases with increasing difference between $\overline{D}_x$ and $\overline{D}_y$ and with increasing distance of *m* from 1, above or below (including negatives). An exception for *m* = 0 is also included to represent twice the geometric mean of $\overline{D}_x$ and $\overline{D}_y$ (i.e. $2 \cdot \sqrt[2]{\overline{D}_x \cdot \overline{D}_y}$).

The laminar generalised mean, $SL_{\overline{D}_x,\overline{D}_y}$ as in Equation (7), is used for the transition term, because it yields the best results in practice. Equation (5) then becomes:

$$\varphi' = Exp\left(\ln(0.5) \cdot \left(\frac{SL_{\overline{D}_x,\overline{D}_y}}{\lambda_k}\right)^{\propto}\right) = 0.5^{\left(\frac{SL_{\overline{D}_x,\overline{D}_y}}{\lambda_k}\right)^{\propto}} \tag{9}$$

The final form of the kernel (see Figure 4 for an example) is then:

$$\beta_T \cdot \left(\frac{\beta_L}{\beta_T} \cdot \varphi' \cdot (SL_{\overline{D}_x,\overline{D}_y})^3 + (1-\varphi') \cdot \frac{(ST_{\overline{D}_x,\overline{D}_y})^2}{Min(\overline{D}_x,\overline{D}_y)} \cdot \left(1 - \frac{(ST_{\overline{D}_x,\overline{D}_y})^2}{\lambda_g^2}\right)\right) \tag{10}$$

with $ST_{\overline{D}_x,\overline{D}_y} \leq \lambda_g$

Since β_T has been factored out as an overall tuning parameter, the original turbulent term is not obtained by simply entering zero for β_L / β_T, because the term is still multiplied by $(1 - \varphi')$. This transition term gives an extra dimension to the turbulent term which was found to be useful in obtaining better PSD accuracy under turbulent conditions. To obtain the original expressions for laminar or turbulent flow regimes, one would input a value for λ_k well above or well below the modelled PSD size range, with a high sharpness α, in order to exclude the effect of the transition.

Figures 1 – 4 present 3-dimensional visualisations of the various kernels described herein, plotted on a log-log size bin scale for the interacting particle sizes.

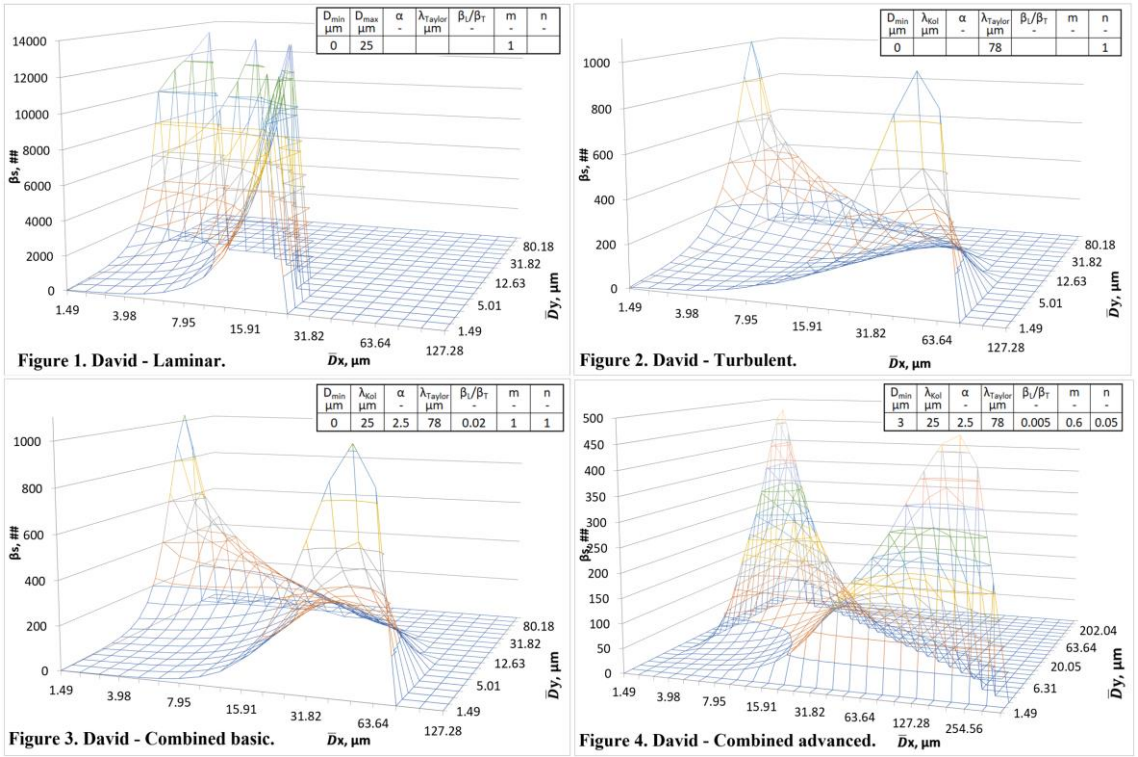

Figures 1–4. 3D representation of various agglomeration kernels.

The use of generalised means provides additional flexibility to the kernel, resulting in better fits between model PSD and actual plant PSD. By using the two additional parameters *n* and *m* the two "mountains" of the kernel and the "valley and ridge" in-between can be shaped to the most suitable fit by affecting the concavity or convexity of the plot when viewed from above. For low values of *n*, the effective maximum doublet size $\overline{D}_x + \overline{D}_y$ of a small plus a large particle is stretched considerably beyond λ_g, as seen in Figure 4 where the mountains are wider and less steep. From calibration experience, the unmodified kernel (Figure 3) tends to overstate the preference of large particles to agglomerate with small particles. Application of the generalised mean in the final form allows for regulation of this effect. The value for *n* is typically around zero.

This kernel is the product of a semi-empirical approach to describing very complex interactions between particles in a tank where different hydrodynamic conditions exist, e.g. being much more different in the vicinity of an agitator than around the inlet of a riser pipe, or between the inside of a draft tube and the annulus of a tank. Changes in scale thickness and fluid viscosity also have their effect. This kernel allows the most suitable parameters values to be selected for each individual tank. How this calibration is accomplished is discussed in Section 4.

2.6 Minimum Participating Diameter

Despite the fact that this combined kernel has a relatively small percentage of fines consumed compared with some other kernels, the disappearance of fines was often still too large as they quickly grew out of their narrow size bins. Increased nucleation could not be used to compensate for this, since it led to distortion and imbalance in particle count. Although Lee at al. [7] found a possible, but statistically not significant trend that smaller gibbsite crystals have smaller growth rates than larger crystals, Misra and White [8] and Ilievski [9] demonstrated that gibbsite growth rate is size-independent, in line with the McCabe ΔL law. Adhering to the latter conclusion, an optional minimum size for agglomeration was introduced. A typical value would be in the order of 3 μm. This aspect is still under scrutiny and will be addressed in further development work.

3. The Modelling Environment

3.1 Particle Size Intervals

SysCAD applies the agglomeration arithmetic developed by Hounslow et al. [10]. This arithmetic assumes that the particles are spherical and distributed over a series of bins with a geometric progression of $\sqrt[3]{2} \cdot D$. As such, the top diameter of bin(x + 1) is $\sqrt[3]{2}$ times the top diameter of bin(*x*). Hence, the corresponding particle volume of bin(x + 1) is twice the particle volume of bin(*x*). The PSD outputs of instrumentation that count particle sizes individually, based on electrozone sensing technique, also follow this sequence. For these studies they are the preferred (but more involved) PSD measuring technique. Lower detection size limit for this equipment is approximately 1 μm.

The top size of the smallest bin in SysCAD is usually 1 or 2μm for Bayer precipitation modelling. It is often useful to define a bin series that includes common industry measurements, such as 45 μm, 90 μm and 22.5 μm. A typical starting size for such sequence would then be ~2.2323 μm.

The starting diameter of the bin size sequence is selected such that the top diameter of the lowest fraction of plant PSD data (usually from routine sampling) corresponds with the top diameter of the first usable bin. Routinely reported PSDs often do not include data below ~ 5 μm because of sample treatment/measuring practices, such as using just Fraunhofer laser diffraction. In such cases it is suggested to extrapolate PSD data into the smaller size bins to account for these particles.

3.2 Agglomeration Simulation

The effect of agglomeration on the change in particle concentration N_x in bin(x) has been described by Hounslow et al. [10] as:

$$\frac{dN_x}{dt} = N_{x-1} \cdot \sum_{y=1}^{x-2} 2^{y-x+1} \cdot \beta_{x-1,y} \cdot N_y + \frac{1}{2} \cdot \beta_{x-1,x-1} \cdot N_{x-1}^2 - N_x \cdot \sum_{y=1}^{x-1} 2^{y-x} \cdot \beta_{x,y} \cdot N_y - N_x \cdot \sum_{y=x}^{\infty} \beta_{x,y} \cdot N_y \quad (11)$$

where:

Nx, Ny Particle numbers in bin(x) or (y) per volume unit or slurry mass unit.

$\beta_{x,y}$ Rate of agglomerate formation between a particle from bin(x) and from bin(y).

The first two terms in Equation (11) represent the number of births into bin(x) resulting from collisions involving particles in the bins below bin(x). The last two terms represent the number of deaths from bin(x) resulting from collisions between particles in bin(x) and particles of all other bins, including those in bin(x) itself. The change in the overall PSD is the result of the simultaneous solution of this equation for each bin. Depending on e.g. the value of λ_g, there are typically around twenty such equations to be solved simultaneously, corresponding to the number of participating size bins.

Hounslow et al. [10] have used volume as the internal coordinate in arriving at Equation (11). Within a bin the particles are evenly distributed on a volume basis, i.e. $\frac{dN}{dV}$ is constant over a bin. It can be calculated that the mean particle diameter within a bin on a volume basis is $\overline{\mathrm{D}}_{Vol,x} = \sqrt[3]{1.5} \cdot \mathrm{D}_{x-1}$ and on a surface area basis is $\mathrm{D}_{Area,x}$ = Sqrt[$\frac{3}{5} \cdot (2^{5/3} - 1)$] $\cdot \mathrm{D}_{x-1}$ with D_{x-1} being the top size of the underlying bin(i-1). Although not specified in [10], arguably $\overline{\mathrm{D}}_i = \sqrt[3]{1.5} \cdot \mathrm{D}_{x-1}$ should be used when applying size-dependent kernels. However, normally the arithmetic mean or geometric mean, $\sqrt[2]{D_{x-1} \cdot D_x}$, is used, as is done in SysCAD.

3.3 Nucleation Simulation

The fine particles generated in simulation of nucleation represent a mixture of genuine nuclei, small agglomerates of nuclei and broken-off crystal chips. In precipitation modelling, SysCAD keeps the smallest index bin, bin(0), empty by moving any material in this bin up into the first usable bin, bin(1). As such, newly generated fines are created directly in bin(1). The nucleation rate is an apparent nucleation rate. Its value is a result of the calibration process discussed hereafter. Johnston and Cresswell [11] used an apparent nucleation rate as well in modelling precipitation. In their model the starting diameter was 10 μm.

3.4 Growth Simulation

The solids mass in a precipitator increases through growth and secondary nucleation. The latter is accounted for separately. Growth increases particles mass without changing particle numbers. Models without PSD simply assume one large bin containing uniform spherical particles and let these particles grow from one specific surface area to the next. In PSD mode there are of course multiple bins. Growth is then realised by moving particles from lower bins to higher bins. It has been a challenge for mathematicians to closely align the arithmetic of such discretising of growth, where surface area is the internal coordinate, with the arithmetic of agglomeration, where volume is the internal coordinate. Hounslow et al. [10] developed an equation for discretising growth, as did Rod Stephenson for SysCAD [12]. These methods, Equations (12) and (13), agree quite well.

M.J. Hounslow:

$$\frac{dN_x}{dt} = \frac{2G}{(1+r)\cdot D_{x-1}}\left(\frac{r}{r^2-1}\cdot N_{x-1} + N_x + \frac{r}{r^2-1}\cdot N_{x+1}\right) \quad (12)$$

R. Stephenson:

$$\frac{dN_x}{dt} = \frac{6G}{\overline{D}_x}\cdot\left(\frac{1}{r}\cdot N_{x-1} - N_x\right). \quad (13)$$

where:

r	$\sqrt[3]{2}$
G	Radial growth rate, µm h^{-1}
D_{x-1}	Lower diameter of bin(x), µm
$\overline{D}_x$	Average diameter of bin(x), µm
x	Bin index > 1. For x = 1 different equations apply.

4. Calibration

The starting point in calibration is a database with (sanitised) daily average process data plus feed and discharge PSDs for a number of precipitators in the circuit over a significant period of time.

Calibration proceeds through two phases:

1. Find the optimum values for the kernel parameters of each tank, or each series of tanks, using the normal operating values (or average values) for process parameters and PSDs over the chosen time period (Base Case). In this process, simultaneously, the associated agglomeration rate b, nucleation rate (#/L/h) and growth rate (µm/h) are found for the Base Case. Note that these rates are not the result of any scientific equations, but purely the result of mass balances, particle count balances and PSD fitting exercises.
2. Find the relationship of agglomeration rate, nucleation rate and growth rate with such process variables as supersaturation, temperature and solids concentration. It is possible to establish such relationships from scratch using the precipitation circuit as a real-life laboratory yielding empirical relationships. However, it is more practical to use established equations. This is not always straightforward, as discussed in Section 5.

The process of calibrating a tank or series of tanks in the model includes two calculation loops: an inner loop of iterations, which can be automated, and an outer loop, which requires user interaction. Within the inner loop, three calibration PID controllers are used simultaneously to meet three objectives/criteria:

1. Match the tank discharge A/C of the model with that of the plant through variation of the growth rate. This ensures that the solids mass balance is satisfied.
2. Match the tank discharge particle count per gram of solids (ppg) of the model with that of the plant through variation of the nucleation rate. This ensures that the solids particle count balance is satisfied.
3. Match the tank discharge -45 µm (%) of the model with that of the plant through variation of the agglomeration rate term (β). This ensures that the frequently-used measure for agglomeration efficiency, (-45 µm (%)$_{feed}$– - 45 µm (%)$_{prod}$) / - 45 µm (%)$_{feed}$ [13], is met between model and plant. This does not say anything about the shape of the PSD yet.

The inner loop produces a PSD that is consistent with these three criteria. Subsequently, this modelled PSD is compared with the real plant PSD to determine its deviation from reality. This is done by automated calculation of the standard deviation of model PSD and plant PSD on a cumulative basis and on a differential basis and taking the average of both. Furthermore, the delta between the product and feed PSDs for the model and plant are graphically overlayed, again both for cumulative and differential PSDs. This is done for visual inspection, and to judge how well the change in PSD over the tank within the model matches the actual change in PSD over the tank in reality: See Figures 5 and 6 for examples of these calibration curves.

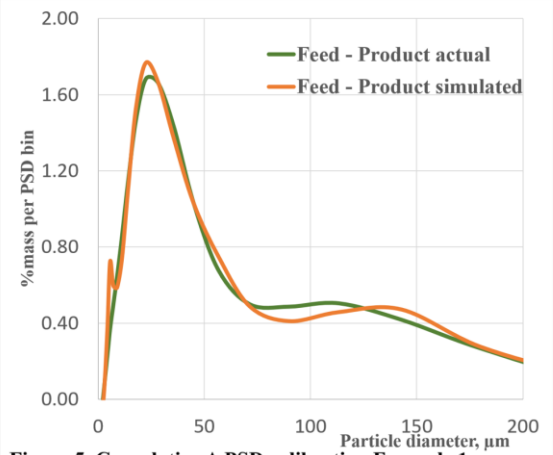

Figure 5. Cumulative Δ PSD calibration Example 1

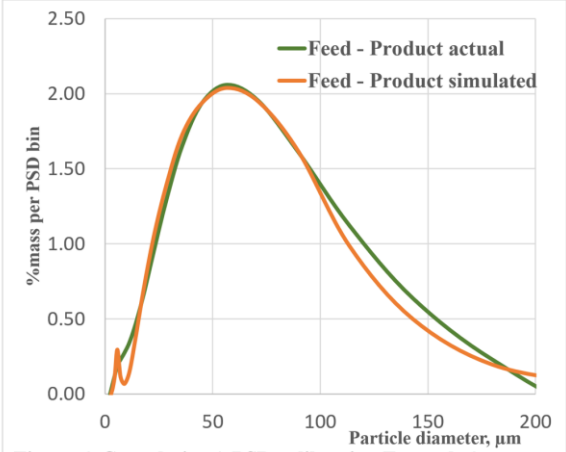

Figure 6. Cumulative Δ PSD calibration Example 2

Figures 5-6. Example delta PSD calibration curves.

In the outer loop of the calibration, the various kernel parameters are manually adjusted in such a way that the change in PSD between feed and discharge for the model and plant match as closely as possible. Using the same procedure, various other kernels have been evaluated with actual plant data. These included Levich [14, 15] and Livk & Ilievski [1]. The closest approach was clearly and convincingly obtained with the new combination kernel, as formulated in Equation (10). Optimum values found were typically in the following ranges:

λ_k: 15 – 50 µm, λ_g: 70 – 80 µm, α: 2 – 4, m: 0.5 – 0.7, n: 0 – 0.1, β_L/β_T: 0

$\beta_L/\beta_T = 0$ means that the original laminar kernel component of the new kernel was not active, but the transition term $(1 - \phi')$ acted in its place.

Simultaneous to the kernel parameters, the average values for growth rate, nucleation rate and agglomeration rate are established, as they are the final results of the inner loop once the optimum set of kernel parameters has been found. The growth rate is calculated from the volume of gibbsite yield in the tank less the yield attributable to nucleation, divided by the total surface area calculated from the tank PSD in the model. The nucleation rate and agglomerate rate are then the rates attributed to the most appropriate set of kernel parameters yielding a PSD that best matches that of the plant. The growth, nucleation, and agglomeration rates are subsequently used together with the associated process parameters, such as temperature and supersaturation, in the user-selected scientific equations to calculate the rate constants that belong to these equations in order to predict these rates under different process conditions.

There are limitations to each of the many rate equations available in the literature. The selected equations may be improved upon, or even developed, through sensitivity analyses using the data in said process database, as discussed in the following Section 5. This especially applies to the supersaturation term used in the growth rate equation and the growth rate term used in the agglomeration rate kernel β. The Base Case is represented by the results of the above calibration exercise on the overall averages of process data across the selected time period.

A point of attention is whether the above exercise produces unique values for nucleation rate and agglomeration rate. In theory, it would be possible to obtain a plant PSD curve in the model using different combinations of nucleation and agglomeration rates if one were unrestrained in selecting different values for agglomeration efficiency independently per bin. In reality, such freedom does not exist. The agglomeration efficiency per bin and the sequence from bin to bin is largely constrained by the general shape of the size kernel, based on scientifically developed equations. With this new kernel there is only one set of kernel parameters, one agglomeration rate and one nucleation rate that yield the closest fit between model and field PSD.

5. Dependencies on Process Conditions

By running a series of test cases on individual precipitators whereby process parameters are varied, or by selecting the appropriate records from a process database, the dependencies of the different rates (e.g. agglomeration rate) on various process parameters may be established. These process parameters include solids concentration, temperature, growth rate or supersaturation, and liquor viscosity. In these cases, the size kernel parameters determined through earlier calibration are kept constant. Agglomeration, nucleation, and growth rates for each sensitivity case are exported to a spreadsheet along with the varied parameters and other conditions of interest. By sorting rate results per parameter, a rough first-pass correlation between rates and parameters can be established through regression. By interlinking these correlations, the effect of a parameter on the correlation of another parameter can be filtered out such that genuine correlations between rates and parameters emerge.

In principle, these rates can be correlated to plant-measurable variables if a sufficiently large database is developed. However, for certain variables, such as growth rate, it is easier to make use of equations that researchers have developed. That said, there are, for example, a wide range of equations for growth rate based on different definitions of supersaturation. An overview of growth rate equations is presented by Li et al. in [16].

Like agglomeration, gibbsite growth was also the subject of a collaborative research program under the umbrella of AMIRA, around the turn of the century. A few years later, with some overlap, Chantal Sweegers [19, 31] conducted a PhD study regarding the morphology and growth kinetics of gibbsite crystals. These and some spinoff studies have contributed significantly to the understanding of the kinetics of gibbsite growth, but still some aspects remain unclear.

5.1 Supersaturation

Growth rate equations generally consist of a supersaturation term σ, an Arrhenius term (temperature dependency) and rate constant, which may include dependency on factors such as liquor impurities. The supersaturation term represents the thermodynamic driving force of the chemical reaction that takes place. There is general agreement that the overall reaction can be written as:

$$Al(OH)_4^-(aq) = \gamma Al(OH)_3(s) + OH^-(aq) \quad (14)$$

Aluminate ions and hydroxyl ions have been identified as major constituents of Bayer liquor. At increased caustic concentration they form ion pairs with sodium ions. Ion pairing with sodium ions is stronger with aluminate ions than with hydroxyl ions [17]. Aluminate ions also form soluble polymeric or oligomeric complexes. An example is the dimer $(OH)_3Al - O - Al(OH)_3^-$, believed to be the Moolenaar's dimer [18], which may constitute up 30 % of the alumina in Bayer liquor, and with which the aluminate ions are in equilibrium. It is very likely that gibbsite precipitation proceeds through such complexes. However, there is only limited knowledge about their roles in precipitation and about their thermodynamic activities in Bayer liquor.

The thermodynamic driving force for the precipitation reaction is the difference in chemical potential between the participating species in solution on the reactant side and the product side. The chemical potential μ_i of species i in solution is defined as:

$$\mu_i = \mu_i^o + RT \cdot \ln(a_i) \quad (15)$$

where:

a_i Product of activity coefficient γ_i and mol concentration $[x_i]$ of species i.

If Equation (14) is considered to be the dominant reaction and the involvement of any other species in the liquor is ignored, then the driving force σ equals:

$$\frac{\Delta\mu}{kT} = \ln\left(\frac{a_{Al(OH)_4^-}}{a_{Al(OH)_{4,eq}^-}}\right) - \ln\left(\frac{a_{OH^-}}{a_{OH_{eq}^-}}\right) = \ln\left(\frac{a_{Al(OH)_4^-}}{a_{Al(OH)_{4,eq}^-}} \cdot \frac{a_{OH_{eq}^-}}{a_{OH^-}}\right) \tag{16}$$

When the ratio of activity coefficients of aluminate over hydroxyl ions is assumed to stay constant during the reaction, then the driving force, and there with the supersaturation term, can be approximated by:

$$\sigma = \ \sigma' = \frac{\Delta\mu}{kT} \approx \ln\left(\left(\frac{[Al(OH)_4^-]}{[OH^-]}\right) / \left(\frac{[Al(OH)_4^-]_{eq}}{[OH^-]_{eq}}\right)\right) \tag{17}$$

Sweegers et al. [19] used Equation (17) in their research into gibbsite growth rate. The expression looks similar to the one used by Cornell et al. [20], except that their expression, $\sigma'' = \ln(A/A_{eq})$, does not include the chemical potential of the hydroxyl ions.

For low supersaturations (σ < 10 %) the following mathematical simplification can be applied:

$$\frac{\Delta\mu}{kT} \approx \ln\left(1 + \frac{\Delta\mu}{kT}\right) \tag{18}$$

After using the above simplification and conversion to North American notation of Bayer liquor concentrations, Equation (17) becomes:

$$\sigma_{simple} = \left(\frac{A}{FC} - \frac{A_{eq}}{FC_{eq}}\right) / \frac{A_{eq}}{FC_{eq}} \quad \text{for } \sigma < 10\ \% \tag{19}$$

where:

A	Alumina concentration, g L^{-1}
FC	Free Caustic concentration, g L^{-1}

However, the supersaturations in the general practice of the alumina industry by far exceed the limit of 10 % for which the mathematical simplification in Equation (19) provides. Supersaturation values greater than 100% are not unusual. Most of the rate equations tabled in [16] use *(A – A_{eq})*, or variants thereof, in the supersaturation term. Therefore, in principle they differ considerably from their thermodynamically more correct logarithmic equivalents. Cornell et al. [20] does use a logarithm term: $\sigma'' = \ln(A/A_{eq})$. This was presented in 1999 as the supersaturation term in the new Alcoa growth rate equation. The power (exponent) of σ'' for the rate equation was found to be 3, which is confirmed by Li et al. [16] who found 2.86 with this form of σ. Sweegers et al. [19], using Equation (17) for σ, found the power to be in the range of 4.5 to 6.7. The supersaturation power of the other rate equations on the basis of *(A – A_{eq})*, or variants thereof, is generally 2, which agrees with the findings of Li et al. [16], who found values in the order of 2.1–2.2.

It has been stated by others, e.g. Ilievski [21], that a supersaturation driving force derived from differences in chemical potential of reaction participating species is theoretically correct, but that it is of little use if the ionic speciation, solution structure and activity coefficients of reacting species are not well known. The absence of such knowledge justified the use of traditional expressions for supersaturation.

Veesler and Boistelle [22] also used Equation (17) as a starting point, but they removed the logarithm and eliminated the hydroxyl concentrations for reason that the NaOH concentrations

are not too different between supersaturated and saturated solutions. This yielded a normalised, non-dimensional $\sigma_{norm} = A / A_{eq}$. They recognised that most authors dealing with gibbsite crystallization use $(A - A_{eq})$ and observed that this term for supersaturation is dependent on caustic concentration and temperature via A_{eq} and, hence, is less practical in use. In their testwork in 1994 [23], they found that the caustic dependency can be eliminated by dividing by A_{eq}. They proposed a second formulation for supersaturation in which the traditional formulation is normalised: $\sigma_{vsl} = (A - A_{eq}) / A_{eq}$. Since that time, the latter expression has been used in many crystallographic studies including the aforementioned collaborative AMIRA research program into gibbsite growth. In those studies σ_{vsl} was referred to as "relative supersaturation".

In their investigations into growth rate, Vernon et al. [18] found, contrary to Veesler and Boistelle, a strong dependency of σ_{vsl} on caustic concentration. Sodium ions were found to play a significant role, reducing the growth rate considerably at elevated caustic concentration. They covered a wider range of caustic concentrations than Veesler and Boistelle had done. Vernon et al. concluded that σ_{vsl} is still an empirical factor, only loosely associated with the true driving force for the precipitation reaction.

In summary, it appears that the expressions for supersaturation as driving force, as commonly used by industry and researchers in rate equations, are essentially empirical expressions.

5.2 Growth Rate

There is general consensus that gibbsite growth rate is surface integration controlled rather than diffusion controlled [24]. Surface integration requires that the tetrahedral coordination of a $Al(OH)_4^-$ unit in solution somewhere along the reaction chain converts to octahedral coordination to fit into the gibbsite lattice. It was established that this is a rapid process, and therefore not rate determining [25]. This also applies to the breaking of the Na^+ $Al(OH)_4^-$ ion pair. There is consensus that the gibbsite surface is likely deprotonated in the highly alkaline environment of Bayer liquor (pH > 14). Since the gibbsite lattice consists of hydrogen bonded layers of $Al(OH)_3$, reprotonation could be a rate determining step, but testwork with the hydrogen isotope deuterium indicated that this is not the case [26]. Sodium ions are adsorbed onto the negatively charged deprotonated gibbsite surface. Vernon et al. [24] observed that the rate constant for gibbsite growth decreases as the sodium ion concentration increases. They also saw that the kinetics and morphology of gibbsite growth alters when sodium ions are replaced by potassium or caesium ions. Based on these observations, Vernon et al. suggest that the rate of sodium desorption from the gibbsite surface controls the rate of integration.

Growth rates vary between the different types of gibbsite crystal faces, of which various morphologies exist. In generalised terms, they usually have basal (hexagonal) top faces and prismatic (usually rectangular) side faces. Vernon et al. [24] found that high caustic concentrations lead to blocky crystals and low caustic concentrations to somewhat elongated (less blocky) crystals, thus with the basal faces then growing faster than the prismatic faces. Furthermore, there is a slight effect of supersaturation on the relative growth rates of basal and prismatic faces. Consequently, the overall growth rate has a certain dependency on the ratio of basal/prismatic face area exposed to the liquor. This is also influenced by agglomeration, where there appears to be a tendency for agglomeration to take place between the prismatic faces [27], leading to a relative overexposure of the basal faces.

Growth rate is also dependent on the type of growth regime. Lee at al. [7] concluded that, at low to medium supersaturation, spiral growth is the growth mechanism on both the prismatic and basal faces. Growth is initiated by crystal defects ("kinks") on the surface, from where a growth front deposits a smooth layer of precipitate on the crystal surface in a continuous fashion. This growth

mechanism, also called screw dislocation, is often referred to as BCF growth (Burton-Cabrera-Frank) for which the following formula applies [28, 16, 26]:

$$G = A_1 \cdot \sigma^2 \cdot \tanh\frac{A_2}{\sigma} \tag{20}$$

where:

A_1, A_2 Complex temperature-dependent constants.

At low supersaturations the tanh term is approximately 1, thus the spiral growth rate is proportional to σ^2 and at high supersaturations it is proportional to σ. Since the gibbsite growth rate at low to moderate supersaturations, up to σ_{vsl} = 0.81, is proportional to the relative supersaturation squared, Lee et al. concluded that spiral growth is the applicable growth mechanism. This conclusion applied to both basal and prismatic faces. Above σ_{vsl} = 0.81, growth on the basal face follows a birth and spread regime. Friej et al. [29] supported this conclusion through Atomic Force Microscope (AFM) observations, at least for the basal face. Brown [30] observed a 2D nucleation growth mechanism on the prismatic faces in industrial, impure liquor. Sweegers et al. [31] used AFM as well, but could not confirm that spiral growth is of any great significance and concluded that two forms of nucleation growth, namely birth and spread, and contact nucleation, are more likely candidates. Sweegers et al. [19] contested the validity of using the squared relationship of the empirical relative supersaturation σ_{vsl} as proof that spiral growth mechanism of Equation (20) applies, since σ would not be the same as σ_{vsl} (as described in Section 5.1).

2D nucleation growth is another well-known form of layered growth. This type of growth is initiated by nuclei formed on the surface from where lateral growth over the surface occurs. There are various growth expressions published for 2D nucleation [16] including for continuous birth and spread. One of those expressions for the latter is [28, 26, 7]:

$$G = B_1 \cdot \sigma^{5/6} \cdot e^{\frac{-B_2}{\sigma}} \tag{21}$$

where:

B_1, B_2 System related constants.

According to Lee et al. [7] spiral growth is the normal growth regime on all crystal faces, except that at higher supersaturations growth on the basal faces changes to continuous birth and spread. The transition point is at σ_{vsl} = 0.81. In their range of data for birth and spread, the supersaturation power z in a rate equation $G = k \cdot \sigma_{vsl}^z$ is calculated to be 2.6. In a plot of G versus σ_{vsl} for the {110} prismatic face, the slope of the curve progressively increases with increasing σ_{vsl}. From σ_{vsl} = 0.8 onwards, a power z of 2.9 for the first segment and 4.8 for the second segment is calculated. This does not agree with Equation (20) for spiral growth where the value for z cannot be greater than 2 and should progressively reduce with σ rather than increase. The conclusion that spiral growth applies to the prismatic face at moderate supersaturations is thus questionable.

Sweegers et al. [31] obtained strong indication that an enhanced formation of 2D nuclei via contact nucleation is one of the growth mechanisms occurring. Contact nucleation was often observed in the case of agglomerates. The edges of two adjacent crystals in contact would act as step sources by lowering the activation barrier for 2D nucleation. Also, steep hillocks in the vicinity of crystal edges suggest contact nucleation. Contact nucleation is the formation of nuclei on the crystal surface through collision of a growing crystal with the tank wall, agitator blade or other crystals. Garside's [28] overview of industrial crystallisation describes it as the most

significant secondary nucleation mechanism in crystallisers handling materials of high or moderate solubility.

The studies discussed so far were microscopic studies. Li et al. [16] performed batch experiments in a stirred tank reactor. Their plotted data shows that below a critical supersaturation, growth rate has an approximately 2nd order dependency on σ_{vsl}, while above this critical supersaturation an approximately 4th order dependency is applicable, suggesting a 2D polynuclear growth. This was only obtained for 55 and 60 °C since at the higher temperatures this critical supersaturation was not reached. Furthermore, Vernon et al. [24] concluded that a nuclear birth and spread type mechanism dominates in agglomeration tanks, while emphasizing that still a lot is unknown. They remarked that an interface layer between liquor and crystal surface, detected and examined by Addai-Mensah et al. [27] appears to play an important role in the creation of growth units.

The important conclusion of this review is that, regardless of the true identity of the growth mechanisms on the various faces under different conditions, different growth rate equations apply for high and moderate-to-low supersaturations. At high supersaturations, the exponent of the supersaturation term as used in its traditional form, based on $(A - A_{eq})$, is variable and markedly greater than 2. This has significant bearing on agglomeration modelling, since growth rate and/or supersaturation are factors in agglomeration efficiency calculations.

In SysCAD, a flexible growth rate equation is available based on the White-Bateman supersaturation term, $(A - A_{eq})/C$, for which the supersaturation exponent can be freely specified for each tank. The exponent is simply determined by plotting ln(G) versus ln(σ) for plant data sorted on said supersaturation term at approximately constant temperature.

5.3 Nucleation Rate

The nucleation rate expression developed by Misra [32] is commonly applied:

$$\frac{dN_0}{dt} = k_{nucl} \cdot (A - A_{eq})^2 \cdot SSAL \qquad (22)$$

where:

$\frac{dN_0}{dt}$	Nucleation rate, # L^{-1}
k_{nucl}	Temperature dependent constant.
$SSAL$	Surface area exposed to liquor, m^2 L^{-1}

In his PhD thesis, Misra [32] assumed the supersaturation power to be 2, in analogy with that for growth rate. But he also remarked that it was difficult to establish a more precise exponent due to the scatter of results. He stated in his thesis that the runs at 40, 45 and 50 °C can be better represented by assuming a 4th power of the supersaturation term. This seems to agree with the observation by Li et al. [16] that supersaturation dependency under conditions where 2D nucleation definitely occurs is approximately 4th order.

Nucleation rate increases with reducing temperature. In Equation (22) this temperature effect is included in k_{nucl}. An Arrhenius term is missing. However, the data presented in the thesis allows estimating the activation energy, which works out to be -54 kJ/mol.

The effect of agitator power input and hydrodynamic conditions are also accounted for in k_{nuel}, thus its value, established through calibration, depends on the tank conditions. Solid phase oxalate (SPO), especially in needle form, is an excellent substrate for gibbsite secondary nucleation [33, 41], thus in co-precipitation circuits SPO also makes a large contribution to secondary nucleation.

5.4 Agglomeration Rate

Agglomeration relies on nucleation type growth, notably contact nucleation growth. From published graphs with data from experimental work by Ilievski and Livk, it is calculated that the agglomeration rate β is proportional to σ_{vsl} to the power of approximately 6 in [34] and approximately 5.6 in [1], at 80 °C. The AMIRA project reported that the power is in the range of 4 to 5, the latter at high supersaturation. In 1991 Ilievski [35] found a 4th order dependency on supersaturation for agglomeration rate, as did Halfon and Kaliaguine in 1976 [36]. Johnston et al. [11] obtained a best fit with a 2nd order dependency.

Agglomeration rate kernels predominantly show a linear proportionality with growth rate [1, 10]. The growth responsible for creating and enhancing the bond between two agglomerating particles is a nucleation type growth such as contact nucleation [31]. The growth regime for layered growth may be a different type of 2D nucleation growth, or, within constraints, spiral growth [7]. Therefore, the overall growth rate measured may indeed be different from the growth rate for agglomeration alone. Thus, if G (overall, as measured) is used in β the power of G may be different from 1. SysCAD allows specifying the power of G in the agglomeration rate term of the kernel. Because different growth mechanisms with their associated growth rates can coexist, the preferable approach may be relating agglomeration rate to supersaturation instead of growth rate and including a separate Arrhenius term to account for the (positive) effect of temperature.

Too high values for growth rate and supersaturation lead to over-agglomeration: oddly shaped aggregates are formed that are susceptible to breakdown, leading to an increased attrition index. Therefore, an optimum value for growth rate (or supersaturation) exists in the balance between agglomeration rate and hydrate strength.

Conclusions on the effect of solids concentration Cs on β differ between researchers. Ilievski and Livk [34] found, with uncertainty, that Cs may have a small negative effect. The data from batch agglomeration tests by Johnston et al. [11] show an inverse relationship between β and Cs. They concluded that doubling the mass of seed charge halved the agglomeration rate, but did not report if the associated reduction in supersaturation had been accounted for. A distinction is sometimes made in the literature between Free-in-Space and Restricted-in-Space collisions [37]. The latter applies to high slurry densities whereby particles only interact with particles in their immediate vicinity. In such case β is inversely proportional with the total particle count. This effectively corresponds approximately with an inverse proportionality with Cs. Free-in-Space is the model mode exclusively seen in alumina-related research papers. The slurries are usually not dense enough to cause much restriction on particle motion. But on the basis of the Restricted-in-Space theory a certain modest downward correction with Cs may be justified.

It is probably not a coincidence that, for constant supersaturation, with increasing temperature the rate of agglomeration increases and the degree of soda occlusion reduces. Both are well-established facts. Grocott and Rosenberg [38] propose that sodium ions become occluded if they are not allowed sufficient time to diffuse away from the growing hydrate surface. They also conclude that these sodium ions do not come directly from the liquor. This coincides with findings by Sang [39] and Ohkawa [40] that caustic concentration has no significant influence on soda occlusion. Caustic concentration does not have a clear influence on agglomeration rate [34]. Thus, it appears that at high pH, regardless the caustic concentration, the growing hydrate surface has a particular concentration of adsorbed sodium ions (see Section 5.2).

The desorption and/or diffusion of these sodium ions away from the interfaces plays a crucial role in soda occlusion and, by inference, also on agglomeration rate. Possibly the strength of the freshly formed hydrate bond between two particles is inversely related to the percentage of soda

occluded. A higher temperature promotes the rate of sodium desorption and diffusion. It may explain why, at temperatures below 65 °C, nucleation primarily takes place with no agglomeration, despite the high growth rates.

5.5 Calibration Observations

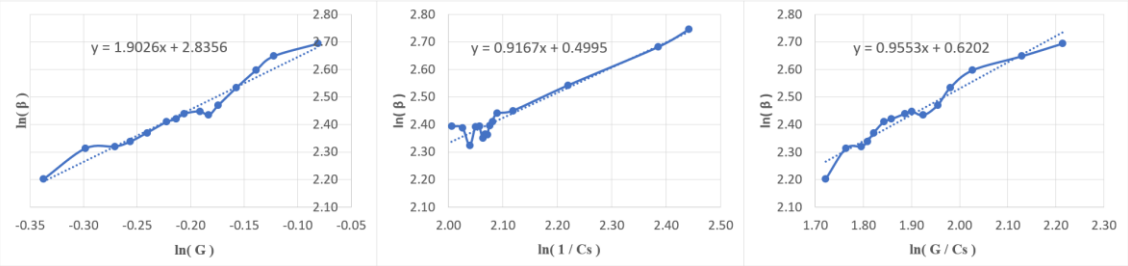

Figure 7. Agglomeration rate (β) sensitivity for growth rate (G) and solids concentration (Cs) in a plant agglomerator.

For establishing the dependency of growth, nucleation and agglomeration rates on process parameters, a procedure has been described earlier in this Section for sorting parameters, performing regression analyses, and interlinking correlations to filter out cross-parameter effects. This procedure is generally successful, but may be difficult if two parameters are strongly correlated. This is the case with growth rate *G* and solids concentration *Cs*. The procedure, applied to data from the agglomeration section of a plant, showed that agglomeration rate correlated strongly with *G* to the power of approximately 2, but at the same time there was a strong correlation between *G* and 1 / *Cs*. This is not surprising. Agglomeration control through seed charge variation is based on this same principle. With insufficient variation or deviation in the latter correlation, it becomes difficult to separate one from the other; see Figure 7 for results on one agglomerator. The dependency of β may as well be with *G* / *Cs* instead of with G^2. The ln (β) versus ln (*G* / *Cs*) plot in Figure 7 produced a power of 0.96 on the *G* / *Cs* term in the expression for β. The same plots for two other agglomerators produced powers of 0.72 and 1.09. Note that *G* is not based on a formula, but calculated from a solids mass balance, as per the calibration procedure described in Section 4. It is the overall *G* resulting from a *G* primarily responsible for growth and a *G* primarily responsible for agglomeration, as discussed in Section 5.4. Since Livk and Ilievski [1] found that the effect of *Cs* on β is small, one would tend to believe that the power of *G* is probably greater than 1, which may be explained on the basis of *G* being a composite of these terms. This subject calls for further investigation.

6. Conclusion

The newly implemented agglomeration kernel in SysCAD, in combination with an advanced calibration procedure, allows tailor-made calibration of PSD development within each tank of a precipitation circuit. It has been developed from a plant process engineer's perspective by focusing on practical application in real-world precipitation circuits, as to get useable answers to important questions concerning process control, design and optimisation. This also applies to the growth rate equation. Different growth regimes exist within a precipitation circuit requiring different exponents on the supersaturation term of the growth rate equation, e.g. with higher values in the agglomeration tank section than in the growth tank section. SysCAD accommodates using different supersaturation powers in the growth rate equation. This is particularly useful because growth rate is a parameter in the agglomeration rate kernel (β). The form in which growth rate should be included in agglomeration kernels still poses some unanswered questions, which will likely be answered in the course of further application of the new kernel and its calibration method in the field.

7. References

1. I.Livk, D.Ilievski, A macroscopic agglomeration kernel model for gibbsite precipitation in turbulent and laminar flows, *Chemical Engineering Science*, 62 (2007), 3787-3797.
2. René David et al., Modelling of multiple-mechanism agglomeration in a crystallization process, *Powder Technology, Elsevier*, (2003), 338-344.
3. René David et al., Developments in the understanding and modeling of the agglomeration of suspended crystals in crystallization from solutions, *Kona*, No.21 (2003), 40-53.
4. René David et al, Crystallization and precipitation engineering – III. A discrete formulation of the agglomeration rate of crystals in a crystallization process, *Chemical Engineering Science*, Vol.46 (1991), 205-213.
5. Andrey Kolmogorov, Dissipation of energy in locally isotropic turbulence, *Doklady Academy of Science*, USSR (1941), 16-18.
6. M.V.Smoluchowski, Versuch einer mathematischen Theorie der Koagulationskinetik Kolloider Lösungen, *Zeitschrift fur Physikalische Chemie*, (1917), 129-168.
7. Mei-yin Lee, Gordon M. Parkinson, Growth rates of gibbsite single crystals determined using in situ optical microscopy, *Journal of Crystal Growth*, (1999), 270-274.
8. C.Misra, E.T.White, Kinetics of Crystallisation of aluminium trihydroxide from seeded caustic aluminate solutions, *Chem. Eng. Prog. Symposium*, Series 67 (1971), 53-65.
9. D.Ilievski, E.T.White, Agglomeration during precipitation: Agglomeration mechanism identification for $Al(OH)_3$ crystals in stirred caustic aluminate solutions, *Chemical Engineering Science*, (1994), 3227-3239.
10. M.J.Hounslow, R.L.Ryall, V.R.Marshall, A discretized population balance for nucleation, growth, and aggregation, *AICHE Journal*, Vol.34, No.11 (November 1988), 1821-1832.
11. R.R.M.Johnston, P.J.Cresswell, Modelling alumina precipitation: dynamic solution of the population balance equation, *Proc. Fourth Alumina Quality Workshop*, (1996), 282-290.
12. Rod Stephenson, A quasi-implicit algorithm for solution of steady state and dynamic particle balance models, *Unpublished paper from poster session at the Ninth Alumina Quality Workshop*, (2012), available on request.
13. O.Tschamper, Improvements by the new Alusuisse process for producing coarse aluminum hydrate in the Bayer process, *Proc. AIME Light Metals Conference*, (1981), 103-115.
14. V.G.Levich, The theory of coagulation of colloids in turbulent liquid stream, *Dokl. Akad. Nauk SSSR*, Vol.99 (1954), 809-812.
15. D.N.Seneviratne et al, An investigation of Bayer desilication product agglomeration mechanism by kernel function population balance modelling, *Proc. Eleventh Alumina Quality Workshop*, (2018).
16. T.S.Li, I.Livk, D.Ilievski, Supersaturation and temperature dependency of gibbsite growth in laminar and turbulent flows, *Journal of Crystal Growth*, 258 (2003), 409-419.
17. H.R.Watling et al, Ionic structure in caustic aluminate solutions and the precipitation of gibbsite, *J. Chem. Soc. Dalton Trans.*, (1998), 3911-3917.
18. C.F.Vernon, G.M.Parkinson, D.Lau, Towards a fundamental rate equation for gibbsite growth in Bayer liquors, *Proc. Fifth Alumina Quality Workshop*, (1999), 129-139.
19. C.Sweegers et al., Growth rate analysis of gibbsite single crystals growing from aqueous sodium aluminate solutions, *Crystal Growth & Design*, Vol. 4, No. 1 (2004), 185-198.
20. R.M.Cornell et al., Precipitation of gibbsite: Development of a new rate equation, *Proc. Fifth Alumina Quality Workshop*, (1999), 153-161.
21. Dean Ilievski, Can gibbsite precipitation be modelled from first principles ?, *Proc. Fourth Alumina Quality Workshop*, (1996), 282-290.
22. S.Veesler, R.Boistelle, About supersaturation and growth rates of hydrargillite $Al(OH)_3$, *Journal of Crystal Growth*, 130 (1993), 411-415.
23. S.Veesler, R.Boistelle, Growth kinetics of hydrargillite $Al(OH)_3$ from caustic soda solutions, *Journal of Crystal Growth*, 142 (1994), 177-183.

24. C.F.Vernon et al, Mechanistic investigations of gibbsite growth, *Proc. Sixth Alumina Quality Workshop*, (2002), 33-39.
25. H.R.Watling et al., IR and ^{27}Al-MAS-NMR spectroscopic studies of sodium(hydroxy)aluminates, *Applied Spectroscopy*, 53-4 (1999), 415-422.
26. Joanne Sook Ching Loh, The role of cations in gibbsite crystallization, *PhD Thesis, Curtin University of Technology*, (January 2001).
27. J.Addai-Mensah, C.A.Prestige, J.Ralston, Interparticle forces, interfacial structure development and agglomeration of gibbsite particles in synthetic Bayer liquors, *Minerals Engineering*, (1999), 655-669.
28. John Garside, Industrial crystallization from solution, *Chemical Engineering Science*, Vol. 40, No. 1 (1985), 3-26.
29. S.Friej et al, Investigation of the growth of gibbsite crystals by atomic force microscopy and optical microscopy, *Proc. Fifth Alumina Quality Workshop*, (1999), 153-161.
30. N.Brown, Secondary nucleation of aluminium trihydroxide in seeded caustic aluminate solutions, Journal of Crystal Growth, (1972), 163-169.
31. C.Sweegers et al, Surface Topography of Gibbsite Crystals grown from Aqueous Sodium Aluminate Solutions, Applied Surface Science, Vol. 187 No. 3-4 (2002), 218-234.
32. C.Misra, The precipitation of Bayer aluminium trihydroxide, PhD Thesis, University of Queensland, (September 1970).
33. M.M.Reyhani et al, Gibbsite nucleation at sodium oxalate surfaces, Proc. Fifth Alumina Quality Workshop, (1999), 181-191.
34. D.Ilievski, I.Livk, An agglomeration efficiency model for gibbsite precipitation in a turbulently stirred vessel, Chemical Engineering Science, (2006), 2010-2022.
35. D.Ilievski, Modelling Al(OH)3 agglomeration during batch and continuous precipitation in supersaturated caustic aluminate solutions, PhD Thesis, University of Queensland, (1991).
36. A.Halfon, S.Kaliaguine, Alumina trihydrate crystallisation. Part 1, Secondary nucleation and growth rate kinetics, Canadian Journal of Chemical Engineering, (1994), 160.
37. D.Green, R.Perry, Modelling and simulation of granulation processes, Perry's Chemical Engineers' Handbook, 8th Edition (2008).
38. S.C.Grocott, S.P.Rosenberg, Sodium in alumina. Possible mechanisms for soda incorporation, Proc. First Alumina Quality Workshop, (1988), 271-287.
39. J.V.Sang, Factors affecting residual soda in precipitation products, Proc. AIME Light Metals Conference, (1988), 147-156.
40. J.Ohkawa, T.Tsuneizumi, T.Hirao, Technology of controlling soda pick-up in alumina trihydrate precipitation, Proc. AIME Light Metals Conference, (1985), 345-366.
41. T.S.Li et al, The influence of solid phase oxalate (SPO) on gibbsite secondary nucleation in synthetic caustic-aluminate solution, Proc. Tenth Alumina Quality Workshop, (2015), 165-173.